Translation and Rotation of Spherulites during the Crystallization of Isotactic Polypropylene with Reduced Chain Entanglements

4 AUTHORS, INCLUDING:

Ziyi Wang
Iowa State University
243 PUBLICATIONS **3,217** CITATIONS

Kaifu Luo
University of Science and Technology of China
44 PUBLICATIONS **1,163** CITATIONS

Yong Huang
Technical Institute of Physics & Chemistry, C…
197 PUBLICATIONS **2,493** CITATIONS

Translation and Rotation of Spherulites during the Crystallization of Isotactic Polypropylene with Reduced Chain Entanglements

Xuehui Wang,[†,‡] Zhigang Wang,*[,†,⊥] Kaifu Luo,[†] and Yong Huang[‡]

[†]CAS Key Laboratory of Soft Matter Chemistry, Department of Polymer Science and Engineering, Hefei National Laboratory for Physical Sciences at the Microscale, University of Science and Technology of China, Hefei, Anhui Province 230026, P. R. China

[‡]State Key Laboratory of Polymer Physics and Chemistry, Beijing National Laboratory for Molecular Sciences, Institute of Chemistry, Chinese Academy of Sciences, Beijing 100190, P. R. China

[⊥]Graduate School, Chinese Academy of Sciences, Beijing 100049, P. R. China

Ⓢ *Supporting Information*

ABSTRACT: The isothermal crystallization of isotactic polypropylene (iPP) spherulites was observed under chain entanglements, reduced chain entanglements, and unconfined thick film conditions using polarized optical microscopy (POM). While spherulite translations and rotations were not observed in entangled iPP samples, the growing spherulites in the entanglements-reduced crystallizing melt conspicuously translated and/or rotated, even when their sizes exceeded the sample film thicknesses. Our entanglements-reduced samples were prepared by first slowly crystallizing a commercial entangled iPP in mineral oil (and then extracting the mineral oil with hexane) and by a direct polymerization method, respectively. The purity of the entanglements-reduced iPP samples and the extent of chain entanglements were examined by thermogravimetric analysis (TGA), gel permeation chromatography (GPC), and rheological measurements. Our findings seem to provide new clues into the crystallization of high molecular mass polymers.
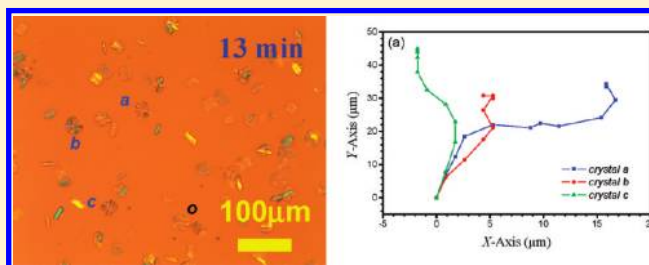
INTRODUCTION

The "tube" or "reptation" picture of chain entanglement introduced by de Gennes[1,2] and Edwards,[3] emphasizing chain localization to a tubelike region defined by surrounding chains, has been further developed by Doi and Edwards[4] and Graessley[5] into an elaborate and predictive theory of high molecular mass dynamic properties of polymer melts. The problem of understanding the crystallization of polymers naturally takes this picture as a starting point since flow, diffusion, and relaxation are all involved in crystallization. Unfortunately, the application of this theory to situations where large deformations are occurring has recently been questioned,[6,7] and there are many unanswered questions about the nature of entangled polymer melts under conditions where there is a large scale flow.

The word "entanglement" is associated with many of the truly remarkable properties of polymers such as their high melt viscosities, shear thinning, transient rubberlike elasticity, and the toughness of many polymer materials.[1] There seems to be clear evidence that the nature of entanglement can somehow be altered substantially under flow, leading to large macroscopically observable effects. For example, Dalnoki-Veress and co-workers[8] observed shear deformation zones in uniaxially strained thin films that depended on the entanglement molecular mass, M_e, which they interpreted as being caused by a reduction of the entanglement density under flow. Escobedo et al.[9] reported a Monte Carlo simulation of an entanglement-free cross-linked polymer network of semiflexible chains indicating a peculiar stepwise elastic response in their model material; similar effects are seen in some tough natural substances. Again some chains in the nature of entanglement under flow seemed to be indicated. Rastogi et al.[10,11] thoroughly studied the heterogeneous distribution of entanglements in polymer melts and its influence on crystallization. They attributed the different characteristics, such as plateau modulus, crystallization rate, etc., to a melt state in which the chain dynamics was altered due to topological constraints, and they did not consider issues of flow associated with crystallization. Of course, the effects of entanglement on the crystallization kinetics of polymeric materials have been much studied because of its practical importance.[12−17]

Our investigation is based on a new singular finding about the nature of polymer crystallization that seems to be tied up with chain entanglement. We have occasionally observed that growing polymer spherulites even with sizes larger than film thickness can translate and/or rotate during isothermal crystallization when the entanglement is reduced (movies are available for this observation in the Supporting Information). What is the cause of this interesting phenomenon, and how can entanglement be involved?

We studied isotactic polypropylene (iPP) without and with a mineral oil treatment that reduced the entanglement density. Time sweep measurement of the storage modulus using a rheometer was made over time, and a stable value was reached after about 20 min, indicating that entanglement density after melting could be maintained in a reduced state for a substantial period of time before the system would become reentangled.[13] This allows us to study the role of reduced entanglements on the crystalline morphology. This phenomenon of entanglement reduction was found when we studied the isothermal crystallization behavior of iPP at moderate supercooling under the unconfined condition (simply crystallizing the film sample with free top surface, i.e., a cover glass was not applied on the sample surface); thus, a negative pressure was not generated to induce flow in the supercooled melt as we have reported in a previous publication.[18] Our measurement simply involves using a polarized optical microscope (POM) to observe the effect of entanglement on the translational and rotational motion of spherulites in polymer films with a free boundary. The entanglements-reduced iPP spherulites translated and/or rotated during their growth while no movement of any kind was found for the entangled iPP spherulite counterpart (see Supporting Information). We discuss possible reasons for this dramatic change in the spherulite growth kinematics.

■ EXPERIMENTAL SECTION

We first studied the crystallization of two fully entangled commercial iPP samples with different molecular masses, iPP1 (purchased from the Sigma-Aldrich Inc., with weight-averaged molecular mass, M_w = 196K, and molecular mass distribution, M_w/M_n = 3.92) and iPP2 (supplied by Beijing Yanshan Petrochemical Co., with M_w = 167K and M_w/M_n = 3.36). Note that gel permeation chromatography (GPC) analysis (Polymer Laboratories, PL-GPC220) was applied to measure the molecular masses and molecular mass distributions for all the iPP samples. Both iPP1 and iPP2 exhibited common polymer crystallization behaviors. To gauge the effect of entanglements on the spherulite growth, we then studied the crystallization of two other types of iPP samples having reduced chain entanglement densities, corresponding to iPP3 (M_w = 199K and M_w/M_n = 3.38) and iPP4 (M_w = 302K and M_w/M_n = 6.71) prepared by two rather different methods. The sample iPP3 was obtained from iPP1 by a physical method, i.e., slow crystallization of iPP1 from its mineral oil solution (at a mass concentration of 5 wt % under vacuum condition)[13] and then extraction of mineral oil with hexane. Thermogravimetric analysis (TGA, PerkinElmer, Pyris 1 TGA) was then applied to examine whether mineral oil was completely removed in iPP3 after precipitation from the mineral oil solution. The sample iPP4 was obtained by a polymerization method, i.e., controlled synthesis using metallocene catalysts, for which the iPP chains crystallized immediately during polymerization, resulting in "disentangled" chains, as inferred operationally from rheological measurements. Specifically, we performed time sweep rheological measurements for all these iPP samples on a rheometer (TA-AR2000, TA Instruments) to detect the storage modulus versus time changes at a fixed frequency of 350 rad/s to examine the extents of reduced chain entanglements. Note that the 350 rad/s frequency was above the crossover point of G' and G'' frequency curves and that was close to the onset of the rubbery plateau regime. At this frequency the storage modulus (elastic) was above the loss modulus (viscous); thus, the re-entanglement process could be easily monitored in time.

Polarized optical microscope (POM, Olympus BX51) was used to observe the isothermal crystallization behaviors for all the iPP samples. The iPP samples were placed between two cover glasses and maintained
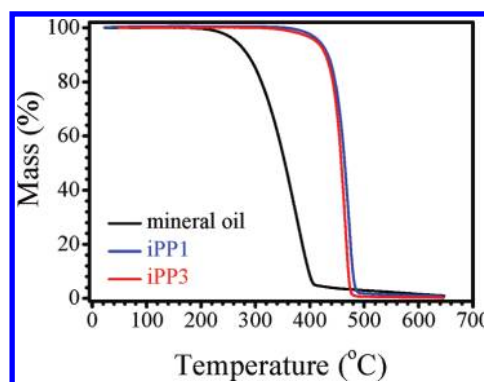

Figure 1. TGA curves of mineral oil, iPP1, and iPP3 at a heating rate of 20 °C/min.

on hot stage at 180 °C for about 30 s before pressed into different thickness films (from 16 to 100 μm) and then quickly quenched to room temperature. The top cover glasses were taken off from the quenched iPP film samples. Note the melting temperatures, T_m, of the iPP samples were about 163 °C (determined by differential scanning calorimetry, DSC, TA series Q200 at a heating rate of 10 °C/min). The iPP film samples having a free top surface were placed on one hot stage at 180 °C for 5 min (to eliminate previous heat history[19]) and then moved to another hot stage kept at 135 °C for isothermal crystallization observation. The crystallization behaviors at other isothermal crystallization temperatures up to 140 °C were also examined. It is emphasized that the isothermal crystallization measurements of iPP samples were made under an unconfined condition; the top iPP film surface was not covered by a cover glass, which is different from our previous study.[13]

■ RESULTS AND DISCUSSION

Before we studied the isothermal crystallization behaviors of the iPP samples, we had to ensure that mineral oil was completely removed from iPP3 since residues of mineral oil could influence the crystallization behaviors. TGA was employed for this purpose. TGA curve of iPP3 is compared with those of mineral oil and iPP1 in Figure 1. The curves were obtained by heating the samples from 25 to 650 °C at a heating rate of 20 °C/min. The results show that mineral oil starts to decompose at about 200 °C and finishes decomposition at a temperature close to 400 °C; iPP1 starts to decompose at 350 °C and finishes decomposition at 490 °C; and iPP3 starts to decompose at 330 °C and finishes decomposition at 480 °C. It can be seen that there is no any signal of decomposition for iPP3 at around 200 °C as mineral oil does, which indicates that mineral oil has been eliminated from iPP3 by using hexane as an efficient extracting agent after the precipitation process. Furthermore, the curve of iPP3 fits quite well with that of iPP1, indicating similar thermal degradation behaviors for these two iPP samples.

Next, we applied the rheological measurements to examine the extents of reduced chain entanglements for iPP3 and iPP4. The iPP1 and iPP2 samples were examined also for comparison purpose. Rastogi et al. have proved the significance of the rheological method for characterization of polymer chain disentanglements and re-entanglements through buildup of the storage modulus with time for the initially disentangled polymer melts.[10,20,21] Theoretically, the average molecular mass between entanglements, M_e, is defined as being inversely proportional to the "entanglement density". It is thus directly related to the elastic modulus in the rubbery plateau region, G_N^0. To follow the
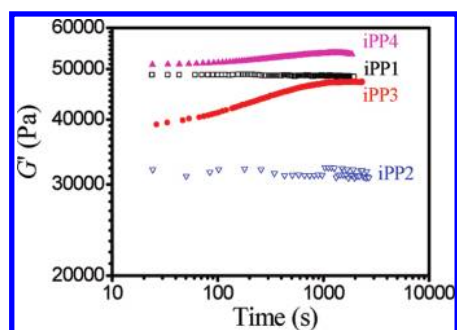
Figure 2. Buildup of storage modulus, G', with time at 180 °C for entanglements-reduced iPP3 and iPP4 melts compared with about constant storage moduli for entangled iPP1 and iPP2 melts.

entanglement evolution in the melt, the change in the apparent plateau modulus with time is estimated via oscillatory shear rheometry using a deformation scale that is characteristic of the linear viscoelastic regime for a material in equilibrium. For polyethylene samples, the plateau modulus region can be reached at above 10 rad/s at 180 °C, and accordingly, Rastogi et al. selected 10 and 100 rad/s frequencies to characterize the evolution of the plateau modulus with time and thus time development of the re-entanglement process for their initially disentangled polyethylene samples.[10,20] The idea of reduced chain entanglements in polymer solutions has been applied to process high-performance commercial fibers of polyethylene (with the trade names Spectra and Dyneema), based on gel-spinning technology invented at DSM in The Netherlands.[22] We found this approach appropriate for our iPP samples. When we prepared iPP3 from iPP1, iPP1 was thoroughly dissolved in mineral oil. The entanglements of iPP1 chains in the solution were reduced significantly compared with the melt state. When iPP1 crystallized from its mineral oil solution during cooling, it is obvious from our experiments that the disentangled chains could be preserved. On the other hand, iPP1 crystallization could further reduce chain entanglements through the chain-folding crystallization process. The reduced chain entanglements in iPP3 and iPP4 are proved by our investigations on the iPP melt rheological behaviors. Crystallization kinetics result of iPP3 also demonstrates its reduced chain entanglements.[13] We note that the plateau region is difficult to reach for our iPP samples. The reasons are as follows: First, the window of rheological measurements of iPP is comparatively small due to a crystallization temperature (145–160 °C) for iPP.[23] Degradation takes place at high temperatures above 240 °C. Second, the plateau zone is more pronounced at higher molecular masses because the terminal relaxation time shifts toward lower frequencies with increasing molecular mass,[23] while the molecular masses of our iPP samples are relatively low. Since it was not possible to measure a significant onset of a plateau zone, the 350 rad/s frequency above the crossover point of $G'-$ and $G''-$frequency curves and close to the onset of a plateau zone was selected. The normal G' and G'' curves as a function of frequency can be found in the Supporting Information. At this frequency the storage modulus (elastic) is above the loss modulus (viscous); thus, the re-entanglement process is more easily probed. A higher frequency also allows more data points to be collected during the early stage of re-entanglement process. A constant strain of 0.3% and a fixed frequency of 350 rad/s were applied in all our measurements. Notably, our measurements were performed in the region close
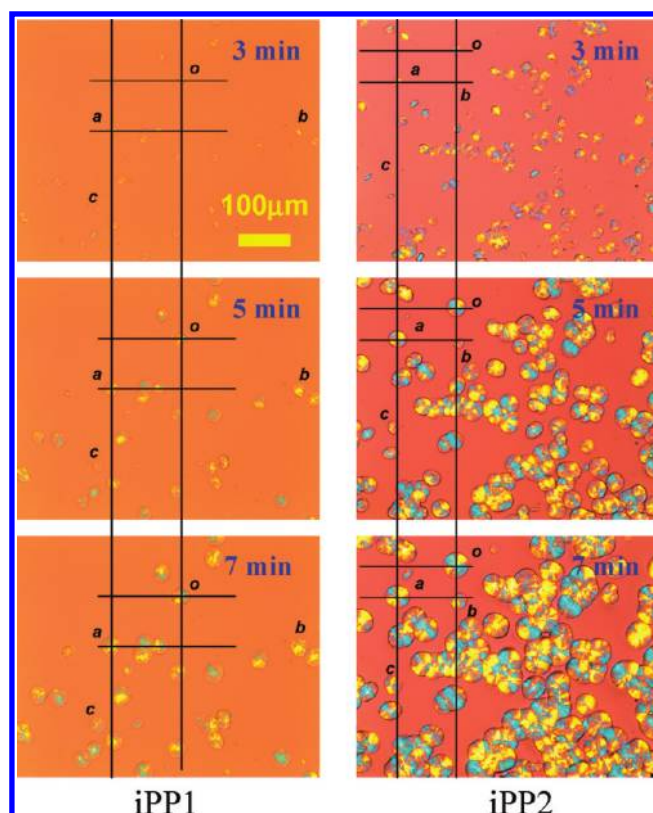

Figure 3. Selected POM micrographs for iPP1 (left panel) and iPP2 (right panel) during isothermal crystallization at 135 °C, indicating none of spherulite translation and rotation. The thickness of the films is 16 μm. The scale bar represents 100 μm and is applied to all the micrographs.

to the rubbery plateau region. The evolution of the storage modulus at the fixed high frequency of 350 rad/s during time sweep measurements for iPP1, iPP2, iPP3, and iPP4 in the molten state at 180 °C is displayed in Figure 2. One significant feature is that no any storage modulus increases are seen for iPP1 and iPP2, while the storage modulus increases with time are seen for iPP3 and iPP4, indicating that the former two samples are fully entangled, while the latter two are entanglements-reduced. At the beginning time, a lower storage modulus is observed for iPP3 compared with iPP1. As the iPP chains tend to mix by themselves and re-entanglements take place during melting, an increase in the storage modulus of about 30% can be obviously observed within the 20 min period. The storage modulus then does not show obvious increase thereafter. The final storage modulus for iPP3 is relatively comparable with that of iPP1. For iPP4 the storage modulus increase is about 6%, less significant than that for iPP3, but the increase is obviously seen. An induction time of about 80 s before buildup of the storage modulus can be found for iPP4, which is due to its high weight-averaged molecular mass (302 K). A similar phenomenon has been reported for buildup of modulus of entanglements-reduced linear polyethylene samples.[20,21] An induction time is absent for iPP3 due to its relatively lower weight-averaged molecular mass (199 K). The late stage storage modulus values for the four iPP samples scale with their weight-averaged molecular masses. Note the late stage storage modulus shown in Figure 2 represents the modulus for each iPP sample at the specific frequency of 350 rad/s used in the study. This modulus (not in the plateau region and
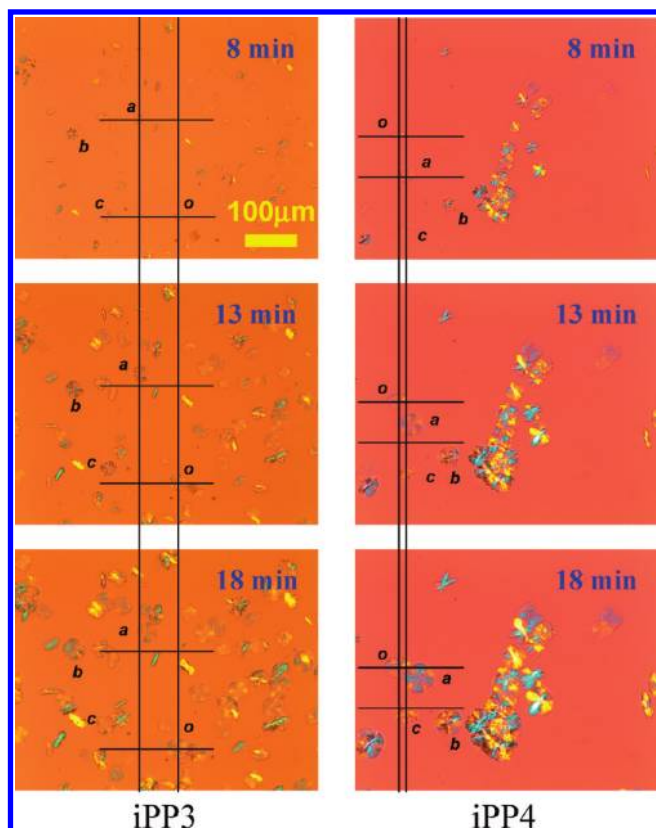
Figure 4. Selected POM micrographs for iPP3 (left panel) and iPP4 (right panel) during isothermal crystallization at 135 °C, indicating spherulite translation. The film thickness is 16 μm for iPP3 and 20 μm for iPP4. The scale bar represents 100 μm and is applied to all the micrographs.

Table 1. Spherulite Sizes (Diameter) for iPP3 and iPP4 during Isothermal Crystallization at 135 °C

time (min)	iPP3 (size in μm)				iPP4 (size in μm)			
	a	*b*	*c*	*o*	*a*	*b*	*c*	*o*
8	19	23	23	25	33	29	25	29
13	31	38	31	35	50	42	38	44
18	44	48	44	42	67	58	54	63

to 5 min or even prolonged times. Recall that the small spherulites in iPP1 and iPP2 films are so abundant that some of them do not initially nucleate from the walls; however, they all keep stationary in terms of nucleation positions no matter where they come from except for growing bigger and bigger. The above result is so common for polymer crystallization that no one even suspects its universality. However, for the isothermal crystallization in iPP3 and iPP4, the entanglements-reduced materials, a different behavior is evident. In the following section we see that in relatively unentangled iPP3 and iPP4 materials spherulites with sizes even larger than the film thickness can both translate and/or rotate, a significantly different crystallization dynamics. Note the measured average spherulite radial growth rate is about 2.6 ± 0.3 μm/min for iPP1 (consistent to our previously published result[13]) and is about 3.7 ± 0.1 μm/min for iPP2. The faster spherulite radial growth rate for iPP2 than iPP1 is due to the lower molecular mass of iPP2 than iPP1.

Figure 4 shows selected POM micrographs of iPP3 and iPP4 during isothermal crystallization, which were taken under the same conditions as for iPP1 and iPP2. Interestingly, we find that during the isothermal crystallization processes of iPP3 and iPP4 some spherulites move (such as the marked spherulite *a*), and some stay in the same places (e.g., spherulite *o*). Compared with the stationary spherulite *o*, spherulite *a* moves about 40 μm distance before becoming fully pinned. This is a big move, barely seen in regular polymer crystallization with fully entangled chains, e.g., iPP1 and iPP2. Several other spherulites move, too, such as the spherulites *b* and *c* (for more other moving spherulites, please watch the movies in the Supporting Information). The trajectories for spherulite centers *a*, *b*, and *c* will be shown later. Again, it is helpful to measure the growing spherulite sizes and compare the sizes with the film thicknesses. For iPP3 and iPP4, the sizes in diameter of spherulites *a, b, c,* and *o* at 8, 13, and 18 min crystallization times are listed in Table 1. It is surprised to find that the spherulite sizes are all larger than the film thicknesses (iPP3 with a thickness of 16 μm and iPP4 of 20 μm). This result infers that the spherulites in fact mainly have two dimensions in the film plane because of the finite film thickness constraint; that is to say, the spherulites very possibly have grown and reached the top surface of the films. However, these "larger than film thickness" spherulites still translate in the film plane. The average spherulite radial growth rate is about 1.3 ± 0.1 μm/min for iPP3 and is about 1.7 ± 0.2 μm/min for iPP4. These spherulite growth rates are relatively lower than the spherulite moving rates in the early stages since the spherulite moving rates show a decay trend with time (shown in Figure 6b). We notice that the spherulite radial growth rate for iPP3 (1.3 μm/min) in this study is obviously lower than that we reported for the same iPP in ref 13 (3.6 μm/min). The difference between these two studies is the experimental design. In ref 13 the sample surfaces were covered by cover glasses for both iPP samples. The difference between the crystallization behaviors

the plateau modulus should be independent from molecular mass[24]) depends on molecular mass, which increases with increasing molecular mass at the same frequency.[25,26]

With the reduced chain entanglements for iPP3 and iPP4 and full entanglements for iPP1 and iPP2 clearly proved, we then continue to demonstrate the corresponding different crystallization behaviors observed by POM for these two categories of iPP samples. Figure 3 outspreads selected POM micrographs for iPP1 and iPP2, which were taken when the samples with 16 μm thickness (top surface is free of cover glass) underwent isothermal crystallization at 135 °C after thermal treatment at 180 °C for 5 min. During the whole isothermal crystallization process, the spherulites of these entangled samples do not move at all. For example, spherulites *o, a, b,* and *c* reside at the same locations during crystallization. This is a common phenomenon observed for polymer crystallization. Since the spherulites form in the thin films between two kinds of walls, with the bottom one the glass substrate and top one the air surface, one may suspect that the spherulite translation and/or rotation are restricted by wall confinements. Thus, we measured the sizes in diameter of the small spherulites, for example, about 8.3 μm for spherulite *b* and 10 μm for spherulite *c* in iPP1 film and 6.3 μm for spherulite *b* and 4.2 μm for spherulite *c* in iPP2 film at the 3 min crystallization time. All the size values are less than the film thickness of 16 μm. The movies available in the Supporting Information for iPP1 and iPP2 do not show any overt translation or rotation for these small spherulites from the beginning time of 2.5 min up
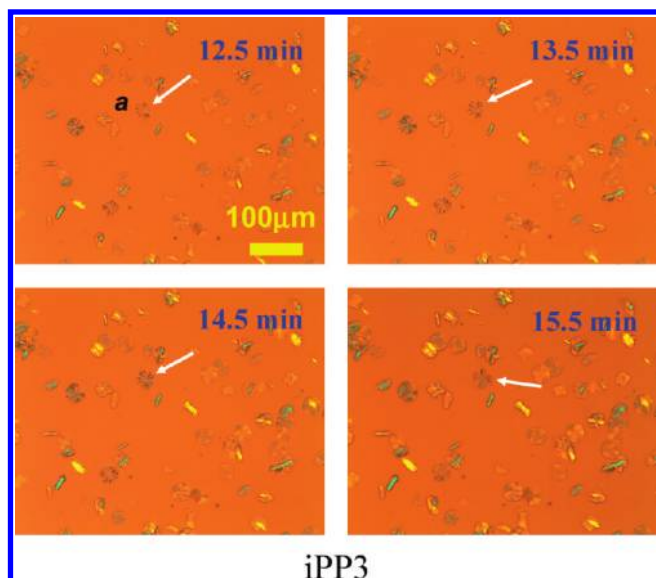
Figure 5. Selected POM micrographs for iPP3 during isothermal crystallization at 135 °C indicating rotation of spherulite *a* (the white arrows demonstrate a clockwise rotation). The film thickness is 16 μm. The scale bar represents 100 μm and is applied to all the micrographs.

in these two studies is the movement of spherulites. In ref 13 the spherulite positions are stationary for both iPP samples. When the spherulites do not move, such as the case of iPP1 (and the commercial iPP sample in ref 13), the spherulite radial growth rate is nearly constant. When the spherulites translate and/or rotate during the growth, such as in iPP3 sample, the radial growth rate is decreased. Further studies are necessary for a rational explanation for this change in kinetics of spherulite growth.

We further find that for entanglements-reduced iPP samples some spherulites not only translate, but they also can rotate! A typical example of this curious phenomenon is depicted in Figure 5 where the rotating spherulite is indicated by a white arrow. (Rotation of other spherulites can be seen in the movies in the Supporting Information.) Note the micrographs were taken under bright field, and the remarked white arrows perpendicularly point at the same lobe of the growing spherulite *a*. Obvious increase of the arrow angle (starting from the vertical direction) indicates that spherulite *a* is rotating with time. The particular angles are 53°, 61°, 65°, and 95° at 12.5, 13.5, 14.5, and 15.5 min crystallization times, respectively. An issue worth mentioning is that for iPP3 some spherulites translate and/or rotate, while some do not. This raises questions about the uniformity of chain entanglement. Rastogi et al. claimed a heterogeneous distribution of entanglements (disentanglements) in the melts.[10,11] We also expect the chain entanglements in our iPP samples exhibit heterogeneity as well.

Figure 6a displays the translating trajectories of spherulites *a*, *b*, and *c* for iPP3 marked in Figure 4. For convenience, we simply take the coordinates of locations of spherulites *a*, *b*, and *c* at 8.5 min crystallization time as (0, 0). As can be seen from Figures 4 and 6a, the three marked spherulites all move. However, they move in different distances and directions depending on the local environments with respect to other growing spherulites. Note the spherulite translation is not caused by temperature gradients from the experimental setup because in that case the spherulite should move in the direction of the temperature gradient. In addition, if a gradient temperature does exist, the entangled iPP
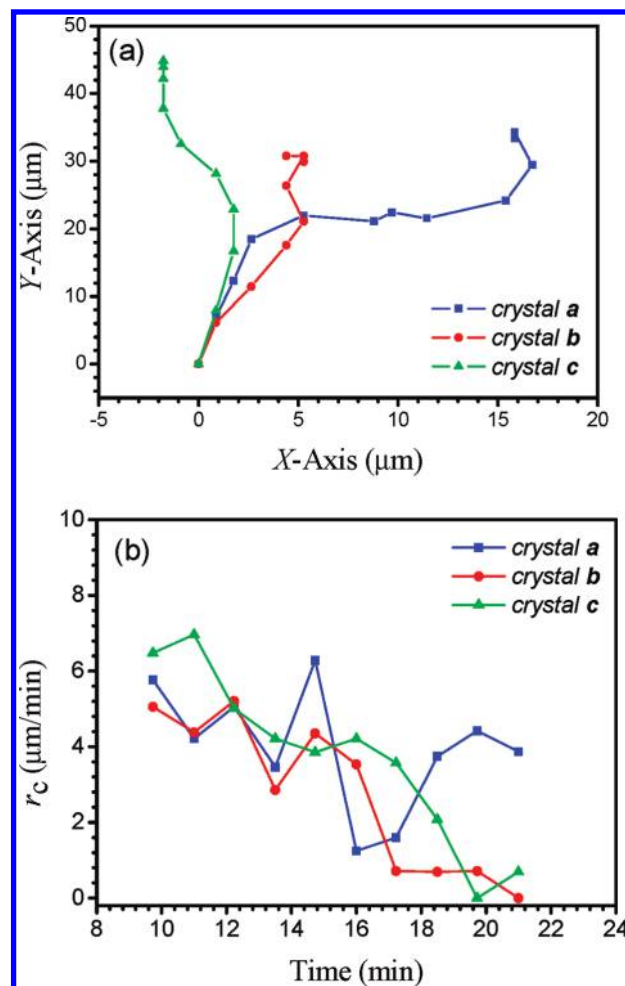

Figure 6. (a) Translating trajectories and (b) displacement rates in two-dimensional film plane of spherulites *a*, *b*, and *c* for iPP3 shown in the left panel of Figure 4.

samples should behave same as the entanglements-reduced samples, but this is not observed. From Figure 6a, the average displacement rates (spherulite moving rates) of the three spherulites can be obtained by taking the averaged displacements after minute intervals. These results are shown in Figure 6b. The displacement rates follow a decreasing trend with local fluctuations. The local fluctuations could be due to different local frictions in the melt in regions where the spherulites translate and/or rotate. For the entanglements-reduced melt, the disentangled regions and entangled regions seem to coexist, and the disentangled regions possess lower local viscosity and higher local mobility than the nearby entangled regions, ultimately causing different local frictions when the moving spherulites run through.[10] In addition, available spare spaces in the film plane are needed for spherulites to move. When the spherulites grow larger and the uncrystallized space becomes reduced, the spherulites begin to move more slowly until finally they freeze through their collective collision. More obvious spherulite moves can be found for iPP4. Figure 7a displays translating trajectories of spherulites *a*, *b*, and *c* for iPP4 marked in Figure 4. Compared with iPP3, within about the same time range, spherulites *a* and *c* move with distances longer than 140 μm (spherulite *c* moves with a distance even longer than 220 μm). Spherulite *b* moves with a short distance since it stops moving when joining with its
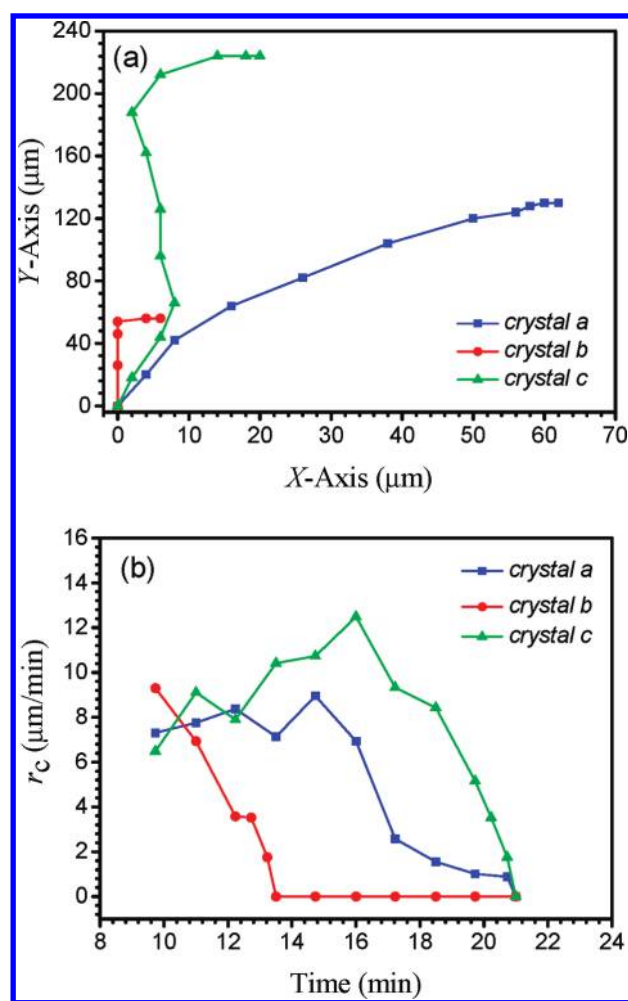
Figure 7. (a) Translating trajectories and (b) displacement rates in two-dimensional film plane of spherulites *a*, *b*, and *c* for iPP4 shown in the right panel of Figure 4.

Table 2. Spherulite Sizes (Diameter) for iPP1 with Film Thickness of 100 μm during Isothermal Crystallization at 135 °C

time (min)	iPP1 (size in μm)			
	a	*b*	*c*	*o*
4	25	38	17	25
8	50	50	49	54
12	79	73	75	81

Table 3. Spherulite Sizes (Diameter) for iPP3 with Film Thickness of 32 μm during Isothermal Crystallization at 135 °C

time (min)	iPP3 (size in μm)			
	a	*b*	*c*	*o*
8	12	20	24	26
13	33	35	41	37
18	43	47	51	49

Our POM results demonstrate that for different sample thicknesses spherulite translation and rotation are always observed for entanglements-reduced iPP3 and iPP4 and are not observed for fully entangled iPP1 and iPP2. For example, for iPP1 with 100 μm film thickness, no any spherulite translation and/or rotation are observed (see a corresponding movie and Figure 2S in the Supporting Information). We emphasize that the early stage spherulite sizes (diameter) in Figure 2S are clearly much smaller than the film thickness (sizes listed in Table 2), but no spherulite translation and/or rotation could be observed for this sample. The stationary nature of the spherulites during growth is obviously not due to the film thickness constraint. The average spherulite radial growth rate for iPP1 of 100 μm thickness is about 3.2 $\pm$ 0.2 μm/min, slightly higher than that for iPP1 of 16 μm thickness (2.6 $\pm$ 0.3 μm/min). We also show in a movie in the Supporting Information that for iPP3 with film thickness of 32 μm (2 times the film thickness of iPP3 in Figure 4) the spherulite translation and rotation can be observed. Figure 3S shows selected POM micrographs for iPP3 with thickness of 32 μm during isothermal crystallization at 135 °C. One stationary spherulite (*o*) and three moving spherulites (*a*, *b*, and *c*) are marked in Figure 3S. The sizes of the four spherulites at the times marked in the micrographs are listed in Table 3. The average spherulite radial growth rate for iPP3 of 32 μm thickness is about 1.4 $\pm$ 0.2 μm/min, similar to that for iPP3 of 16 μm thickness (1.3 $\pm$ 0.1 μm/min), indicating that the film thickness does not affect much on the spherulite radial growth rate. Once again we can see that at 13 and 18 min spherulites *a*, *b*, and *c* all have grown to sizes larger than the film thickness of 32 μm; however, they all move during this period. This result is not surprising since if the spherulites translate and/or rotate in the thinner films (such as 16 μm) they can do the same thing more easily in the thicker ones (from 16 to 100 μm). Figure 4S (see Supporting Information) displays the spherulite center trajectories and displacement rates of spherulites *a*, *b*, and *c* of iPP3 marked in Figure 3S. Compared with the results for the thinner film of 16 μm, the moving distances and displacement rates of the marked spherulites for the thicker film of 32 μm are both increased. Nonetheless, the

right side spherulite aggregates. Larger distance motions for the spherulites in iPP4 are considered to be related to its higher molecular mass because the chain re-entanglements for iPP4 must take a longer induction time and the re-entanglement rate is then relatively slower, as found in Figure 2. This suggests that the spherulite motion has an intrinsic relation with the chain disentanglement state and re-entanglement process. Accordingly, Figure 7b shows the averaged displacement rates of spherulites *a*, *b*, and *c* for iPP4. Spherulite *b* shows a decay displacement rate since it moves a short distance and "senses" its right side spherulite aggregates soon. Nevertheless, the initial displacement rate of spherulite *b* is comparable to that of spherulites *a* and *c*, reaching about 9 μm/min, about 5 times of the spherulite radial growth rate (1.7 $\pm$ 0.2 μm/min). Spherulite *a* moves with about constant displacement rates of 7—8 μm/min within a duration time of 6 min and then gradually slows down as the spherulite begins to collide spherulite *o*. Spherulite *c* moves with a surprisingly increased displacement rates up to about 12 μm/min within a duration time of 6 min and then gradually slows down until finally joining with spherulite *a*. The total moving time for spherulites *a* and *c* is more than 10 min.

The effect of film thickness of iPP samples (from 16 to 100 μm) on the above observed phenomenon was further examined.

overall trends are quite similar regarding to the film thickness influence for iPP3 samples.

POM observations were also performed for the iPP samples at different isothermal crystallization temperatures from 130 to 140 °C. All the results confirm the spherulite translation and rotation for iPP3 and iPP4, but not for iPP1 and iPP2. The question remains as to the nature of the mechanism for spherulite translation and rotation during isothermal crystallization of entanglement-reduced iPP.

First, the spherulite translation and rotation are not caused by any possible temperature gradient because the temperature gradient if existing by any chances should produce similar effects on all these iPP samples. But this is not the case. Second, iPP1 and iPP2 are two fully entangled polymers with difference in molecular mass and exhibit similar behaviors in respect to none of spherulite translation and/or rotation, while iPP3 and iPP4 are two entanglements-reduced polymers with large difference in molecular mass and exhibit similar behaviors in respect to spherulite translation and/or rotation. Evidently, the molecular mass difference by itself is not the cause for the observed spherulite translational and rotational motions. Third, we consider the possible effect of melt flow induced by crystallization as we and others previously reported.[18,27−30] The thought is that the melt flow induced by crystallization might take the spherulites to move together. However, the experimental conditions for these two crystallization systems are quite different. Previous studies on melt flow induced by crystallization were made under a confined condition, while the present study is for an unconfined polymer material. As previously reported, under confinement a large negative hydrostatic pressure can develop during crystallization of melt, which provides an obvious explanation of the driving force for polymer melt flow.[18,27−30] But for the unconfined crystallizing material, as is in the present study, a negative hydrostatic pressure during crystallization should not arise. Galeski et al. have depicted that for thick films with free boundaries local stresses can simply relax at the free surface, and film thinning occurs instead of buildup of a local negative pressure within the film as crystallization occurs.[27−31] Thus, for our case under the unconfined condition no negative hydrostatic pressure exists, which will not be the driving force for melt flow and neither for spherulite translation and/or rotation. Since spherulite movements are only observed for entanglements-reduced iPP compared with the fully entangled iPP, this phenomenon is very possible to originate from the reduced entanglements in the iPP melt matrix. For iPP with fully entangled chains, spherulite translation is limited due to the entangled network-like structure of the matrix; even film thinning is not strong enough to cause spherulite movement. While for iPP with entanglements-reduced chains, the spherulites behave differently. With reduced entanglements, the constraint to spherulite movement becomes reduced. Therefore, we observed the unique spherulite movement in entanglements-reduced iPP during crystallization. Reduced chain entanglements play a key role for spherulite translational and rotational motion.

Finally, to shed some further light on this intriguing phenomenon, we take into account diffusion of iPP spherulites in different local melt environments, namely disentangled versus entangled environments. It is well-known that the mean-squared displacement of a spherulite $\langle X^2(t)\rangle = 6Dt^\alpha$, where D is the diffusion coefficient, t the time, and α the diffusion exponent.[32] The diffusion coefficient $D = k_BT/\xi$, where k_B is the

Boltzmann constant and T the temperature. The frictional coefficient $\xi = 6\pi\eta R$, where η is the melt viscosity and R the diameter of the spherulite. According to $\langle X^2(t)\rangle = (k_BT/\pi\eta R)t^\alpha$, the spherulite translation slows with increased R, reflecting the growing viscous friction and mutual spherulite interaction when they begin to collide to form a solid.

In a disentangled environment with viscosity η_1 (such as iPP3), the mean-squared displacement of a spherulite with diameter $R_1(t)$ is $\langle X_1^2(t)\rangle = (k_BT/\pi\eta_1R_1)t$; here $\alpha = 1$ is used due to the normal diffusion behavior (the Brownian motion). In contrast, the spherulite translation in an entangled environment involves anomalous diffusion where the time exponent α of $\langle X^2(t)\rangle$ is less than 1. (The diffusion coefficient and Stokes law have no meaning under these conditions.) For a spherulite with diameter $R_2(t)$ in an entangled environment with viscosity η_2 (such as iPP1), its diffusion satisfies $\langle X_2^2(t)\rangle = (k_BT/\pi\eta_2R_2)t^\alpha$. Specifically, a spherulite with diameter $R_2(t)$ in an entangled environment with viscosity η_2 exhibits a typical scaling, $\langle X_2^2(t)\rangle \sim t^\alpha$. In the entangled environment, the spherulite can be completely trapped, leading to $\alpha \approx 0$. As a result, $\langle X_2^2(t)\rangle$ does not change with time; that is the reason why we did not observe spherulite movement. The relatively high viscosity in the entangled melt for spherulites is sufficient to explain this effect. On one hand, the size of the spherulite increases with time, which slows its diffusion (see Figures 6b and 7b). On the other hand, once a spherulite meets other spherulites, it can become trapped, and its translation is then greatly reduced, regardless of entanglement. As mentioned before, the disentangled chains in the "entanglements-reduced" melt only occupy a certain portion, and the disentangled chains have a heterogeneous distribution in the melt. Currently, we do not know how to measure the portion of disentangled chains and how to characterize the distribution as well, but from the experimental observation of moves of some spherulites in the "entanglements-reduced" melt in this study we infer that the "disentangled' regions might have a much lower viscosity than those with entangled chains. A quantitative examination of the extent of reduced entanglements and heterogeneous distribution of disentangled chains in the melt by particle tracking, etc., will be pursued in the future.

■ CONCLUSIONS

We have investigated the role of reduced entanglements on the isothermal crystallization behaviors of iPP melts at moderate supercooling under unconfined condition. For entanglements-reduced iPP samples obtained from slow crystallization of a commercial iPP in mineral oil solution with subsequent mineral oil extraction by hexane and controlled synthesis, we observe an interesting phenomenon by using polarized optical microscopy that the *in situ* formed iPP spherulites can translate and/or rotate during isothermal crystallization even when the spherulite sizes grow exceeding the film thickness, whereas no traces of spherulite translation and rotation are observed in its entangled counterpart. This discrepancy is attributed to reduced chain entanglements. This curious spherulite translation and rotation phenomenon has rarely been reported in the literature. It was occasionally observed by us when we studied the effect of reduced entanglements on iPP crystallization behaviors. Further investigations using other polymeric materials will be pursued to confirm its universality.

■ ASSOCIATED CONTENT

ⓢ Supporting Information. Six movie files and one pdf file containing the introduction to the movies, Figure S1 to show changes of storage modulus, G', and loss modulus, G'', with frequency for iPP1 and iPP3 at 180 °C, and Figures S2—S4 to demonstrate influences of iPP film thickness on the spherulite motion. This material is available free of charge via the Internet at http://pubs.acs.org.

■ AUTHOR INFORMATION

Corresponding Author

*E-mail: zgwang2@ustc.edu.cn.

■ ACKNOWLEDGMENT

■ REFERENCES

(1) de Gennes, P.-G. *Scaling Concepts in Polymer Physics*; Cornell University Press: Ithaca, NY, 1979.

(2) de Gennes, P.-G. *J. Chem. Phys.* **1971**, *55*, 572.

(3) Edwards, S. F. *Proc. Phys. Soc.* **1967**, *92*, 9.

(4) Doi, M.; Edwards, S. F. *J. Chem. Soc., Faraday Trans. 2* **1978**, *74*, 1789, 1802, 1818.

(5) Graessley, W. W. In *Macromolecular Conformation and Dynamics of Macromolecules in Condensed Systems*; Nagasawa, N., Ed.; Studies in Polymer Science Series; Elsevier: Amsterdam, 1988; Vol. 2, p 163.

(6) Wang, S. Q.; Ravindranath, S.; Wang, Y. Y.; Boukany, P. *J. Chem. Phys.* **2007**, *127*, 064903.

(7) Wang, S. Q. *Macromolecules* **2007**, *40*, 8684.

(8) Si, L.; Massa, M. V.; Dalnoki-Veress, K.; Brown, H. R.; Jones, R. A. *Phys. Rev. Lett.* **2005**, *94*, 127801.

(9) Bhawe, D. M.; Cohen, C.; Escobedo, F. A. *Phys. Rev. Lett.* **2004**, *93*, 257804.

(10) Rastogi, S.; Lippits, D. R.; Peters, G. W. M.; Graf, R.; Yao, Y.; Spiess, H. W. *Nature Mater.* **2005**, *4*, 635.

(11) Lippits, D. R.; Rastogi, S.; Hohne, G. W. H.; Mezari, B.; Magusin, P. C. M. M. *Macromolecules* **2007**, *40*, 1004.

(12) Robeli-Souffach, E.; Rault, J. *Macromolecules* **1989**, *22*, 3581.

(13) Wang, X. H.; Liu, R.; Wu, M.; Wang, Z. G.; Huang, Y. *Polymer* **2009**, *50*, 5824.

(14) Bu, H.; Gu, F.; Bao, L.; Chen, M. *Macromolecules* **1998**, *31*, 7108.

(15) Sun, Q.; Fu, Q.; Xue, G.; Chen, W. *Macromol. Rapid Commun.* **2001**, *22*, 1182.

(16) Psarski, M.; Piorkowska, E.; Galeski, A. *Macromolecules* **2000**, *33*, 916.

(17) Xu, L.; Fan, Z. Y.; Zhang, H. D.; Bu, H. S. *J. Chem. Phys.* **2002**, *117*, 6331.

(18) Xu, D.; Wang, Z. G.; Douglas, J. F. *Macromolecules* **2007**, *40*, 1799.

(19) Alfonso, G. C.; Ziabicki, A. *Colloid Polym. Sci.* **1995**, *273*, 317.

(20) Lippits, D. R.; Rastogi, S.; Talebi, S.; Bailly, C. *Macromolecules* **2006**, *39*, 8882.

(21) Talebi, S.; Duchateau, R.; Rastogi, S.; Kaschta, J.; Peters, G. W. M.; Lemstra, P. J. *Macromolecules* **2010**, *43*, 2780.

(22) Smith, P.; Lemstra, P. J. *J. Mater. Sci.* **1980**, *15*, 505.

(23) Eckstein, A.; Suhm, J.; Friedrich, C.; Maier, R.-D.; Sassmannshausen, J.; Bochmann, M.; Mu1haupt, R. *Macromolecules* **1998**, *31*, 1335.

(24) Shigeharu Onogi, S.; Masuda, T.; Kitagawa, K. *Macromolecules* **1970**, *3*, 109.

(25) Liu, C. Y.; He, J. S.; van Ruymbeke, E.; Keunings, R.; Bailly, C. *Polymer* **2006**, *47*, 4461.

(26) Wood-Adams, P. M.; Dealy, J. M.; deGroot, A. W.; Redwine, O. D. *Macromolecules* **2000**, *33*, 7489.

(27) Galeski, A.; Koenczoel, L.; Piorkowska, E.; Baer, E. *Nature* **1987**, *325*, 40.

(28) Galeski, A.; Piorkowska, E.; Koenczoel, L.; Baer, E. *J. Polym. Sci., Polym. Phys. Ed.* **1990**, *28*, 1171.

(29) Pawlak, A.; Galeski, A . *J. Polym. Sci., Polym. Phys. Ed.* **1990**, *28*, 1813.

(30) Nowacki, R.; Monasse, B.; Piorkowska, E.; Galeski, A.; Haudin, J. M. *Polymer* **2004**, *45*, 4877.

(31) Nowacki, R.; Kolasinska, J.; Piorkowska, E. *J. Appl. Polym. Sci.* **2001**, *79*, 2439.

(32) Metzler, R.; Klafter, J. *Phys. Rep.* **2000**, *339*, 1.